

DNS study of turbulent transport at low Prandtl numbers in a channel flow

By MARZIO PILLER¹, ENRICO NOBILE¹
AND THOMAS J. HANRATTY²

¹Dipartimento di Ingegneria Navale, del Mare e per l'Ambiente, Sezione di Fisica Tecnica,
Università di Trieste, Via A. Valerio 10, I-34127 Trieste, Italy

²Department of Chemical Engineering, University of Illinois, Urbana, IL 61801, USA

(Received 2 January 2001 and in revised form 28 September 2001)

Direct numerical simulations of the velocity and temperature fields for turbulent flow in a channel are used to examine the influence of Prandtl number Pr on turbulent transport. The Reynolds number, based on the half-height of the channel and the friction velocity, is $Re_\tau = 150$. Prandtl numbers of 1.0, 0.3, 0.1, 0.05, 0.025 were studied. The bottom and the top walls were kept at constant temperatures of $+T_w$ and $-T_w$. The influence of Pr on Reynolds transport, on the turbulent diffusivity, α_t , and on the spectral density function of the temperature fluctuations was studied. The observation that spatial variations of the ratio of the turbulent diffusivity to the value observed at $Pr = 1.0$ are not large is used to propose a method for calculating average temperature fields. The decrease in α_t with decreasing Pr is related to observations of the increased damping of high-wavenumber temperature fluctuations. Molecular conductivity, at smaller Pr , is pictured to act as a filter that renders high-frequency velocity fluctuations ineffective in transporting heat.

1. Introduction

The transport of heat in turbulent fields at small Prandtl numbers is affected by the turbulence in two ways. First, molecular diffusivity plays a more important direct role because it can be of the same order as the turbulent diffusivity. Secondly, molecular motion causes thermal tags to escape from eddies and therefore decreases the effectiveness of the turbulence in mixing. Laboratory studies of the turbulence are very difficult because fluids with large molecular conductivities, such as mercury or liquid sodium, are difficult to handle. This paper reports on a study in which direct numerical simulations (DNS) of turbulent velocity and temperature fields are used. The goals are to define the effect of Prandtl number on statistical properties of the temperature field and on profiles of eddy conductivity, α_t .

The system considered is the fully developed temperature field that would be realized for turbulent flow in a rectangular channel with bottom and top walls maintained at constant temperatures, $+T_w$ and $-T_w$. This provides a simple case since the heat flux is constant across the channel. The Reynolds number is $Re_\tau = Hu_\tau/\nu = 150$, where u_τ is the friction velocity, H is the half-height of the channel, and ν is the kinematic viscosity. Temperature fields characterized by Prandtl numbers Pr of 0.025, 0.05, 0.1, 0.3 and 1.0 were studied.

Several DNS studies have been undertaken in other laboratories, in which both walls of the channel were kept at the same mean temperature. Kim & Moin (1989)

carried out a DNS for $Pr = 0.1, 0.71, \text{ and } 2.0$ at $Re_\tau = 180$. They assumed generation of heat within the fluid and removal of heat at both walls. Calculated profiles of turbulent diffusivity were approximately the same for $Pr = 0.71, 2.0$. However, a significant decrease was found when the Prandtl number decreased from 0.71 to 0.1. Wavenumber spectra were not presented and no attempt was made to develop a correlation for α_t .

Kasagi & Ohtsubo (1993) used a constant heat flux at both walls but allowed the temperature to vary with time and position. Prandtl numbers of 0.71 and 0.025 were studied at $Re_\tau = 150$. They found a decrease in α_τ with decreasing Pr but did not provide a correlation. Their spectral density functions of the temperature fluctuations were plotted in such a way that the definition of the beginning of an inertial–diffusive subrange was not clearly shown. However, they did report that the drop in the spectral density function at large wavenumbers was steeper for $Pr = 0.025$.

Kawamura *et al.* (1998) carried out a DNS of temperature fields at $Re_\tau = 180$ for $Pr = 0.025, 0.05, 0.1, 0.2, 0.4, 0.6, 1.0, 1.5, 5.0$. A constant heat flux was maintained at both walls. They found that the values of α_t for $Pr = 0.6, 0.71, 5.0$ were approximately the same. However, for $Pr < 0.6$ decreases in α_t with decreasing Pr were observed. Wavenumber spectra were not presented.

Theoretical studies have focused mainly on homogeneous isotropic turbulence. Saffman (1960, 1963) and Kontomaris & Hanratty (1993) considered dispersion from a point source and showed how molecular diffusivity decreases the contribution of turbulence. Kontomaris & Hanratty (1994) have presented results from a DNS study which examined the effect of Prandtl number on turbulent dispersion from a point source at the centre of a channel through which a fluid was flowing. Several investigators have examined the effect of Pr on the wavenumber spectrum of the temperature fluctuations in homogeneous, isotropic turbulence (Batchelor 1959; Batchelor, Howells & Townsend 1959; Tennekes & Lumley 1972; Hinze 1975).

A comprehensive experimental study of temperature spectra has been carried out by Clay (1973), over a range of Prandtl numbers of 0.02 to 7, in order to test the theoretical results cited above, as well as scaling arguments presented by Gibson (1968*a, b*).

The main theoretical contribution of this paper is the use of spectral density functions of the fluctuating temperature to provide an interpretation of the observed influence of Prandtl number on the eddy diffusivity and on statistical properties of the fluctuating temperature field. The observation that the ratio of the turbulent diffusivity at a given Prandtl number to the turbulent diffusivity at a Prandtl number of unity is roughly constant over the whole cross-section of the channel, with the exception of $y^+ < 10$, could be useful in making practical calculations.

The work described in this paper is related to a previous study by Na, Papavassiliou & Hanratty (1999) in which the spectral density functions of the scalar field were used to interpret results obtained from DNS studies at $Pr \geq 1$.

2. Theoretical background

2.1. Mean temperature profile

The instantaneous temperature can be defined as the sum of the mean and fluctuating components, $T = \bar{T} + \vartheta$. The contribution of turbulence to the transport of heat is defined as $\rho c_p \overline{v\vartheta}$ where v is the fluctuating velocity component normal to the wall. A fully developed flow is considered. The two walls are kept at constant temperatures

of $+T_w$ and $-T_w$, so the time-averaged heat flux across the channel is independent of location. Therefore,

$$\overline{v\vartheta} - \alpha \frac{d\bar{T}}{dy} = \frac{q}{\rho c_p} = \frac{q_w}{\rho c_p}, \quad (2.1)$$

where q is the local heat flux, q_w is the heat flux at the wall, ρ is the fluid density, c_p is the specific heat capacity, y is the coordinate perpendicular to the wall and $\alpha = k/\rho c_p$ is the molecular diffusivity.

A turbulent diffusivity, α_t , can be defined as

$$\overline{v\vartheta} = -\alpha_t \frac{d\bar{T}}{dy} \quad (2.2)$$

so that (2.1) can be written as

$$-(\alpha + \alpha_t) \frac{d\bar{T}}{dy} = \frac{q}{\rho c_p} = \frac{q_w}{\rho c_p}. \quad (2.3)$$

The integration of (2.3) yields

$$\bar{T}_w - \bar{T} = \int_{-H}^y \frac{q_w}{\rho c_p (\alpha + \alpha_t)} dy \quad (2.4a)$$

and

$$\frac{h_c H}{k} = \frac{1}{\int_{-1}^0 (1 + (\alpha_t/\alpha))^{-1} d(y/H)}, \quad (2.4b)$$

where h_c is a heat-transfer coefficient, defined using $\bar{T}_w - \bar{T}_c$, where \bar{T}_c is the centreline mean temperature. For $\alpha_t = 0$, equation (2.4b) gives $h_c H/k = 1$.

Equation (2.1) can be made dimensionless by using the friction velocity, u_τ , a characteristic length ν/u_τ , and a friction temperature $T^* = q_w/\rho c_p u_\tau$, giving

$$\overline{v^+\vartheta^+} - \frac{1}{Pr} \frac{d\bar{T}^+}{dy^+} = 1. \quad (2.5a)$$

A second way is to use T_w , u_τ and H as normalizing factors:

$$\overline{v^+\vartheta} - \frac{1}{Pe_\tau} \frac{d\bar{T}}{d(y/H)} = \frac{h_c}{u_\tau \rho c_p}. \quad (2.5b)$$

The Reynolds transport terms in (2.5a) and (2.5b) are modelled as

$$\overline{v^+\vartheta^+} = -\frac{\alpha_t}{\nu} \frac{d\bar{T}^+}{dy^+}, \quad \overline{v^+\vartheta} = -\frac{\alpha_t}{Hu_\tau} \frac{d\bar{T}}{d(y/H)}. \quad (2.6a, b)$$

2.2. Spectra

The magnitude of the temperature fluctuations is characterized by their variance, $\overline{\theta^2}$. One-dimensional wavenumber spectral density functions $W_{\vartheta_i}(k_i)$ can be defined as

$$\overline{\theta^2} = \int_0^\infty W_{\vartheta_i}(k_i) dk_i, \quad (2.7)$$

where k_x is a wavenumber in the flow direction, x , and k_z is a wavenumber in the spanwise direction, z . Of particular interest is the influence of Prandtl number on $W_{\vartheta_i}(k_i)$. Theoretical work on this problem has focused on three-dimensional spectra

of scalar fluctuations in a homogeneous, isotropic field. Discussions are presented in books by Hinze (1975) and by Tennekes & Lumley (1972). Even though the flow considered in this paper is inhomogeneous, these theoretical results are considered since they are useful in providing a physical interpretation of spectra that are obtained with the DNS of channel flow.

Kolmogorov has suggested the existence, at large Reynolds numbers, of an equilibrium condition for which the three-dimensional energy spectral density, W , is a function of the dissipation of kinetic energy, ε , the kinematic viscosity, ν , and the wavenumber, k . An inertial subrange is defined by the function

$$W = \gamma \varepsilon^{2/3} k^{-5/3}, \quad (2.8)$$

where $k = (k_x^2 + k_y^2 + k_z^2)^{1/2}$ is the magnitude of the three-dimensional wavenumber. A Kolmogorov microscale is defined as $\eta = (\nu^3/\varepsilon)^{1/4}$. The neglect of the influence of viscosity in (2.8) becomes invalid when k is large compared to η^{-1} .

Hinze (1975) and Tennekes & Lumley (1972) discuss an equilibrium condition at large Reynolds numbers for which the three-dimensional spectral density for temperature fluctuations has the following functionality:

$$W_g = f(\varepsilon, \varepsilon_g, k, \nu, \alpha), \quad (2.9a)$$

where ε_g is the dissipation of $\overline{g^2}/2$. Obukhov (1949) and Corrsin (1951) suggest the existence of an inertial subrange in which the influence of ν and α can be neglected, so that

$$W_g = \beta \varepsilon_g \varepsilon^{-1/3} k^{-5/3}. \quad (2.9b)$$

A thermal microscale is defined as $\eta_g = (\alpha^3/\varepsilon)^{1/4}$. It is seen that $\eta = \eta_g$ for $Pr = 1$. The use of (2.9b) at $Pr < 1$ requires that k is small compared to η_g^{-1} . Clay (1973) considered measurements of velocity and temperature fluctuations in a mercury tunnel, a water tunnel, the ocean, a heated air jet and the atmospheric boundary layer over the ocean and suggested $\beta \approx 0.6$.

The range of wavenumbers for which (2.9b) is valid is called the inertial-convective subrange. An inertial-diffusive subrange can be defined for which W_g depends on α but not on ν :

$$W_g = f(\varepsilon, \varepsilon_g, k, \alpha). \quad (2.10a)$$

This will exist in a range of wavenumbers for which $\eta_g^{-1} < k < \eta^{-1}$. Batchelor *et al.* (1959) consider this subrange by rewriting (2.10a) as

$$W_g = f(W, \varepsilon_g, k, \alpha). \quad (2.10b)$$

Since only W_g and ε_g include the dimension of temperature, equation (2.10b) can be rewritten as

$$W_g = \varepsilon_g f(W, k, \alpha). \quad (2.10c)$$

Batchelor *et al.* also assumed that, in this range of wavenumbers, W_g varies linearly with W :

$$W_g = C \varepsilon_g W \alpha^{-3} k^{-4}, \quad (2.10d)$$

where C is a dimensionless constant. If W is given by (2.8), equation (2.10d) predicts that $W_g \sim k^{-17/3}$. This result has been verified in the studies of temperature spectra in mercury by Clay (1973). It is consistent with other theories in that it predicts an abrupt decrease in W_g at low Pr when $k = O(\eta_g^{-1})$.

One-dimensional spectra are related to three-dimensional spectra by the following

equation, presented in Hinze (1975, p. 285), for a homogeneous isotropic field:

$$E_{g_i}(k_i) = \int_{k_i}^{\infty} dk \frac{E_g(k)}{k}. \quad (2.11)$$

Note that for $k_i \rightarrow \infty$ the one-dimensional spectrum will depend on contributions from $E_g(k)$ at large k . However, for $k_i \rightarrow 0$ the one-dimensional spectrum will depend on contributions from $E_g(k)$ both for small and large wavenumbers. For situations in which $E_g(k)$ is given by a power-law, equation (2.11) predicts that $E_{g_i}(k_i)$ will exhibit the same functionality. Thus equation (2.9b) gives

$$W_{g_i}(k_i) = \frac{3}{5} \beta \varepsilon_g \varepsilon^{-1/3} k_i^{-5/3}. \quad (2.12)$$

3. Numerical procedures

Numerical solutions were obtained for the three-dimensional, time-dependent Navier–Stokes equations in a skew-symmetric form and the advection–diffusion equation. Algorithms, developed by McLaughlin, that are described by Lyons, Hanratty & McLaughlin (1991), were used. In presenting the results, x , y , z and u , v , w represent coordinates and velocity components in the streamwise, the wall-normal and the spanwise directions, respectively.

Results were presented by Lyons *et al.* (1991) for $Pr = 1$ and $Re_\tau = 150$. A $128 \times 65 \times 128$ grid was used in a computational domain of $\lambda_x^+ = 1900$ and $\lambda_z^+ = 950$. The results on the velocity field were substantiated with LDV measurements by Niederschulte, Adrian & Hanratty (1990). Calculated temperature fields compared favourably with laboratory measurements by Corcoran *et al.* (1952) and by Page *et al.* (1952). Results from our laboratory for $Pr = 1, 3, 10$ were recently reported by Na *et al.* (1999). These used a grid of $128 \times 129 \times 128$ for $Pr = 1$ and 3 and of $128 \times 193 \times 128$ for $Pr = 10$. Brooke (1994) used the code of Lyons *et al.* (1991) with a $128 \times 65 \times 128$ grid to calculate temperature fields for $Pr = 0.05, 0.1, 0.3, 0.6$. These results appear in Papavassiliou & Hanratty (1997) and Kasagi & Iida (1999).

The present work uses a grid of $128 \times 129 \times 128$. Some differences were noted from the previous results of Brooke. To a small extent, these arose because of the difference in the resolution in the y -direction. However, a more important factor is that the calculations of Brooke had not converged sufficiently.

4. Results

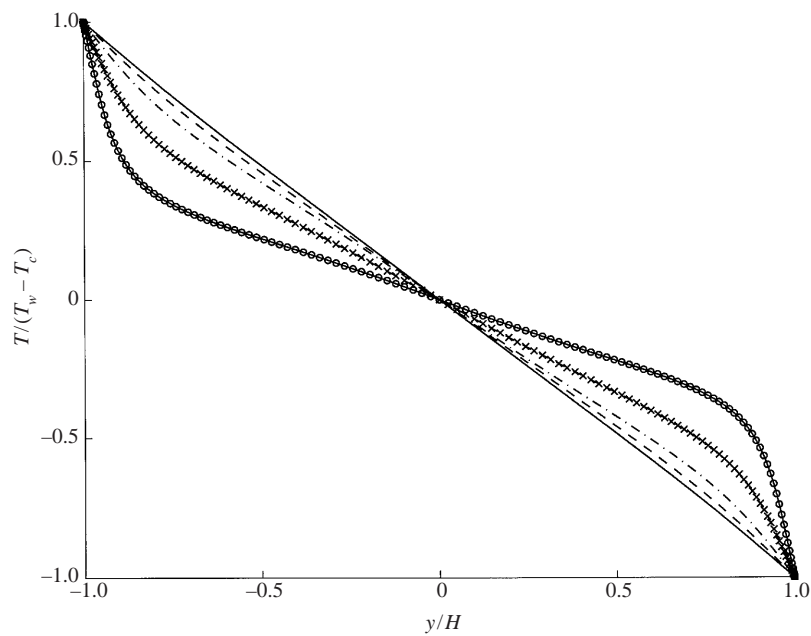
4.1. Profiles of mean temperature

The calculations for which results are presented are summarized in table 1. It includes a listing of the ratio of the ΔT defined using the centreline temperature, $\Delta T = T_w - 0$, and the ΔT that is defined with the bulk average temperature in the bottom half of the channel, $\Delta T = T_w - T_B$.

Calculated local time-mean temperatures, for $Pr = 0.025, 0.05, 0.1, 0.3$ and 1.0 are presented in figure 1. The centre of the channel is defined as $y = 0$ and H is the half-height. The temperature field is fully developed. If the flow were laminar the profile would be a straight line and the heat flux would be $q_w = kT_w/H$. A Péclet number is defined as $Pe_\tau = Hu_\tau/\alpha$, where α is the molecular diffusivity of heat. This Péclet number equals 3.75 for $Pr = 0.025$. The turbulent diffusivity is of the order of $0.03Hu_\tau$ in the central region of the channel for $Pr = 0.025$. Thus, the results for $Pr = 0.025$ and $Re_\tau = 150$ correspond to a ratio of the molecular diffusivity to the

Pr	$\frac{T_w - T_c}{T_w - T_B}$	y_c^+	Nu_B	Nu_c	$\frac{\overline{v^+g^+}}{y^{+3}} \times 10^6$	$\frac{\alpha_t}{\alpha_{t,Pr=1.0}}$
0.025	1.776	23.4	1.95	1.10	8.4	0.38
0.05	1.717	14.3	2.18	1.27	25.4	0.50
0.1	1.642	9.2	2.72	1.65	72.8	0.67
0.3	1.467	5.6	4.40	3.00	237.1	0.84
1.0	1.276	3.7	8.09	6.34	749.9	1.00

TABLE 1. Summary of the calculations.

FIGURE 1. Mean temperature profiles at different values of Pr , at $Re_\tau = 150$. \circ , $Pr = 1.0$; \times , $Pr = 0.3$; $- \cdot -$, $Pr = 0.1$; $- - -$, $Pr = 0.05$; $- - -$, $Pr = 0.025$.

turbulent diffusivity of about 9. Molecular diffusion dominates, so the temperature profile approaches that for a laminar flow.

For $Pr = 1$, the Péclet number is 150. The turbulent diffusivity is of the order $0.08Hu_\tau$, so the ratio of the molecular diffusivity to the turbulent diffusivity for $Pr = 1$, $Re_\tau = 150$ is about 0.08. Therefore, the slope of the temperature profile is much smaller in the centre of the channel than is observed for $Pr = 0.025$. Close to the wall the turbulent diffusivity decreases. Since the heat flux is a constant, independent of y , the slope of the temperature profile increases in the near-wall region. Eventually, a conductive sublayer region is reached very close to the wall where molecular transport dominates. The slope of the profile is the largest here. The profiles show a systematic change from these two asymptotic behaviours for $0.025 \leq Pr \leq 1$.

Temperature profiles are plotted in semi-logarithmic coordinates in figure 2, where the symbols indicate data obtained from DNS calculations. The temperature is made dimensionless with T^* and the distance from the wall, y_w , is scaled with ν/u_τ . The conductive sublayer is defined by the equation $\bar{T}^+ = Pr y^+$. The location where

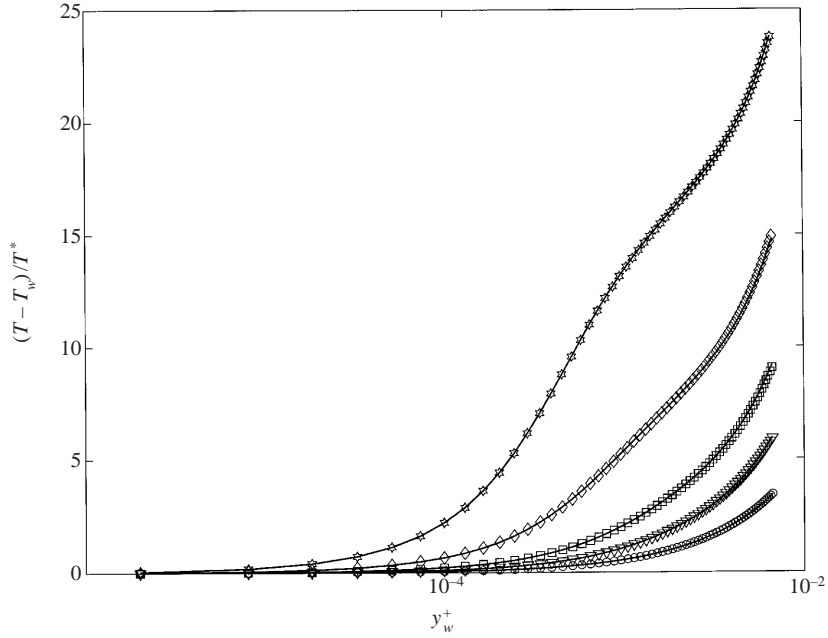


FIGURE 2. Mean temperature profiles at different values of Pr , at $Re_\tau = 150$. The symbols indicate DNS data. The solid curves are calculations that use a proposed model for α_t . Steeper curves correspond to progressively higher Prandtl numbers of 0.025, 0.05, 0.1, 0.3, 1.0.

the temperature profile deviates from this relation by 1% is used by us to define the thickness of the sublayer, y_c^+ . Values of y_c^+ determined in this way are listed in table 1. A logarithmic behaviour is not observed in any of the curves in figure 2, because of the low Re_τ used in the calculations. This is illustrated in figure 3 where $-y^+(d\bar{T}^+/dy^+)$ is plotted against y/H . An extended plateau region does not exist.

Values of the Nusselt number, defined as

$$Nu_c = \frac{q_w H}{(\bar{T}_w - \bar{T}_c)k}, \quad (4.1)$$

are plotted in figure 4 as plus signs and presented in table 1. A very good fitting of the results for Nu_c , in the range $3.75 \leq Pe_\tau \leq 45$, is

$$Nu_c = 0.8905 + 0.0597 Pe_\tau^{0.9361}, \quad (4.2)$$

where $Pe_\tau = Re_\tau Pr$. By expanding equation (2.4b) in a Taylor series, around $Pe_\tau = 0$, it is possible to show that the limiting behaviour of Nu_c for $Pe_\tau \rightarrow 0$ can be represented by

$$Nu_c - 1 = \frac{\partial}{\partial Pe_\tau} \left[\int_{-1}^0 \left(\frac{\alpha_t}{u_\tau H} \right) d\left(\frac{y}{H}\right) \right]_{Pe_\tau=0} Pe_\tau^2. \quad (4.3)$$

Thus, in the limit $Pe_\tau \rightarrow 0$

$$Nu_c - 1 \cong C Pe_\tau^2 \quad (4.4)$$

so empirical equation (4.2) does not capture the correct behaviour for $Pe_\tau \rightarrow 0$. The choice of $C = 0.00685$ allows both the value and the derivative of Nu_c obtained from equations (4.2) and (4.4) to be equal at $Pe_\tau = 3.75$. Note that equations (4.2) and (4.4) imply that the Nusselt number depends on Pe_τ . This hypothesis is sustained

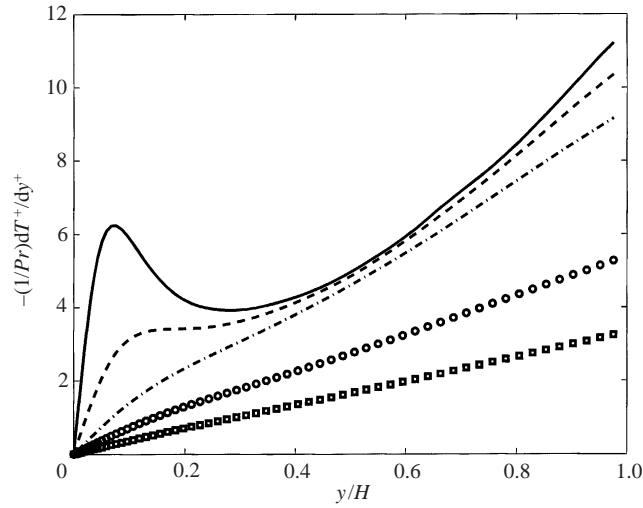


FIGURE 3. Profiles of $-y^+ d\bar{T}^+/dy^+$ at different Prandtl numbers, at $Re_\tau = 150$. \square , $Pr = 0.025$; \circ , $Pr = 0.05$; $-\cdot-$, $Pr = 0.1$; $- -$, $Pr = 0.3$; $-$, $Pr = 1.0$.

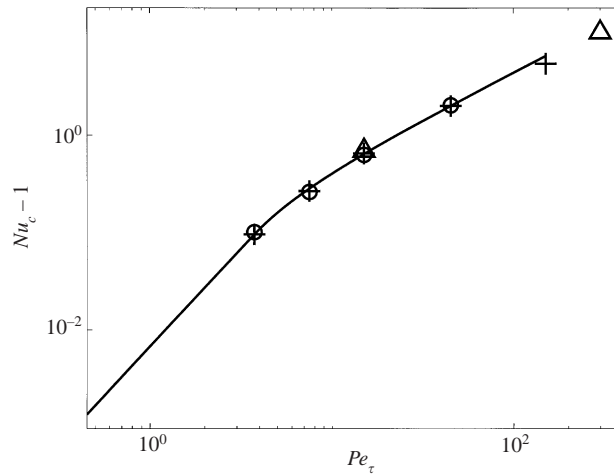


FIGURE 4. Nusselt number, equation (4.1), plotted as function of Pe_τ . DNS data at $Re_\tau = 150$ (+) are compared both with calculations performed by using the proposed model for α_t (\circ) and with equations (4.2) and (4.4) ($-$). Equations (4.2) and (4.4) match both in value and slope at $Pe_\tau = 3.75$. Δ , DNS data obtained at $Re_\tau = 300$, $Pr = 0.05$ and $Pr = 1.0$. The first case corresponds to the same Péclet number obtained at $Re_\tau = 150$ for $Pr = 0.1$.

by the very good agreement between DNS data obtained at the same $Pe_\tau = 15$, for calculations with $Re_\tau = 150$ and 300 , represented by plusses and triangles in figure 4.

Most empirical formulae reported in the literature use the Nusselt number defined as

$$Nu_B = \frac{q_w D_h}{(T_w - T_B)k}, \quad (4.5)$$

with H replaced by the hydraulic diameter both in the Nusselt number, and in the Péclet number, which is defined with bulk velocity rather than u_τ and designated by Pe_B in this paper. For channel flow, the hydraulic diameter equals four times

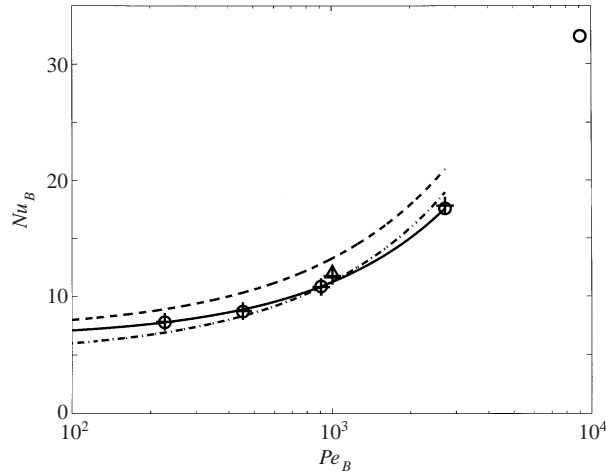


FIGURE 5. Nusselt number, equation (4.5), plotted as function of Pe_B . DNS data at $Re_\tau = 150$ (\circ) are compared both with calculations performed by using our proposed model for α_t ($+$) and with equations (4.6) (—), (4.7) (- - -) and (4.8) (- · - ·). The triangle represents a DNS that was carried out at $Re_\tau = 300$ and $Pr = 0.05$.

the half-height, H . The bulk Reynolds number, evaluated using this length scale, is approximately 9053 for the calculations at $Re_\tau = 150$. Note that Nu_B at $Pe_B = 0$ is a function of the mean velocity field used to define the bulk temperature. For a uniform mean velocity across the whole channel, $Nu_B = 8.0$ at $Pe_B = 0$. For the velocity field used in this paper $Nu_B = 7.24$ at $Pe_B = 0$. Furthermore, in the limit of $Pe \rightarrow 0$, the bulk Nusselt number is not given by an equation of the same form as equation (4.4).

The solid curve in figure 5, given by the equation

$$Nu_B = 6.38 + 0.0153Pe_B^{0.834}, \quad (4.6)$$

fits the calculations for $0 \leq Pr \leq 0.3$ and $Re_\tau = 150$. It does not give the correct value of Nu_B at $Pe_B = 0$ (that is, 7.24). Results from a number of investigations for heat transfer in tubular flows, discussed by Knudsen & Katz (1958), are similar to equation (4.6): for example, Lyons *et al.* suggest that

$$Nu_B = 7.0 + 0.025Pe_B^{0.8} \quad (4.7)$$

and Seban & Shimazaki give

$$Nu_B = 5.0 + 0.025Pe_B^{0.8}. \quad (4.8)$$

These are plotted as the dashed and dot-dashed curves in figure 5, respectively. Rough agreement between (4.6) and (4.7) is noted. This figure also presents calculations for Nu_B performed with our proposed model for α_t . A very good agreement with the DNS data is observed. Moreover, a data point reported from a DNS we are currently carrying out, at $Re_\tau = 300$ and $Pr = 0.05$ (given as a triangle), is close to the curve represented by equation (4.6).

4.2. Reynolds transport and eddy diffusivity

Values of the dimensionless Reynolds transport, $\overline{v^+ \vartheta^+}$, are plotted in figure 6. Strong decreases are observed for decreasing Pr . Since the friction temperature is used to make $\overline{v \vartheta}$ dimensionless the decrease is, to a large extent, due to the increase in T^* (or q_w) with decreasing Pr .

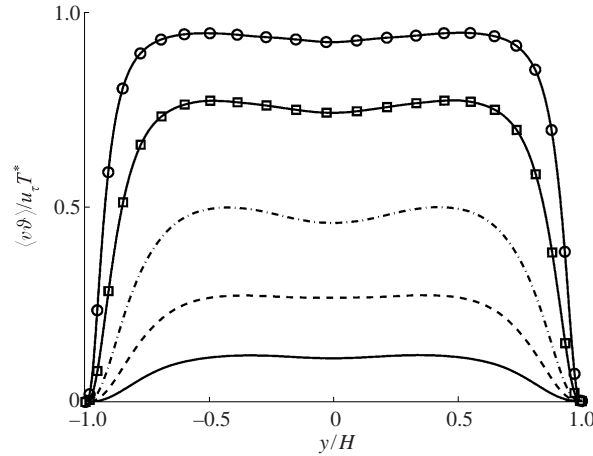


FIGURE 6. Turbulent heat flux, scaled by the friction velocity and the friction temperature. Profiles are reported from DNS calculations at $Re_\tau = 150$, and at various Pr . —, $Pr = 0.025$; ---, $Pr = 0.05$; - · - · -, $Pr = 0.1$; -□-, $Pr = 0.3$; -○-, $Pr = 1.0$.

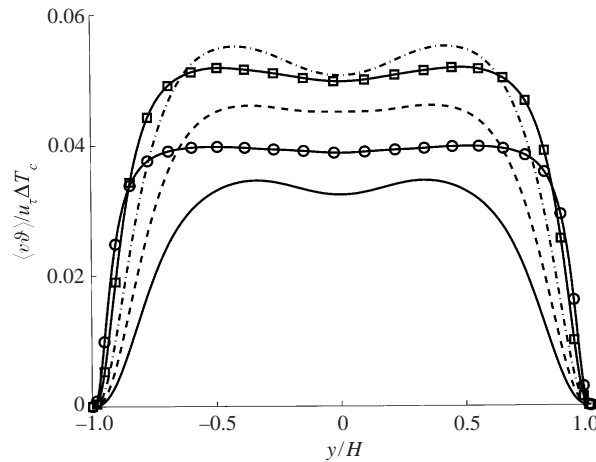


FIGURE 7. Turbulent heat flux, scaled by the friction velocity and the temperature difference between wall and centreline. Profiles are reported from DNS calculations at $Re_\tau = 150$, and at various Pr . —, $Pr = 0.025$; ---, $Pr = 0.05$; - · - · -, $Pr = 0.1$; -□-, $Pr = 0.3$; -○-, $Pr = 1.0$.

This type of plot obscures the influence of Pr in the core region. Therefore, $\overline{v\vartheta}$ is normalized with u_τ and $\Delta \overline{T}_c = T_w$ in figure 7. An interesting behaviour is observed. The non-dimensional $\overline{v\vartheta}$ in the core region is found to increase when Pr decreases from 1 to 0.3. A monotonic decrease is observed at all y/H with a decrease in Pr from 0.1 to 0.025. Clearly Pr is affecting $\overline{v\vartheta}$ in two different ways. A possible explanation for this is explored in the next section. The limiting values of $\overline{v^+\vartheta^+}/y^{+3}$ for $y_w^+ \rightarrow 0$ are summarized in table 1. These show a strong decrease with decreasing Pr . The results for $Pr = 1$ appear to be qualitatively different from the results for lower Pr in that

$$\left. \frac{d}{dy^+} (\overline{v^+\vartheta^+}/y^{+3}) \right|_w > 0$$

and a maximum is observed at $y_w^+ \approx 4$.

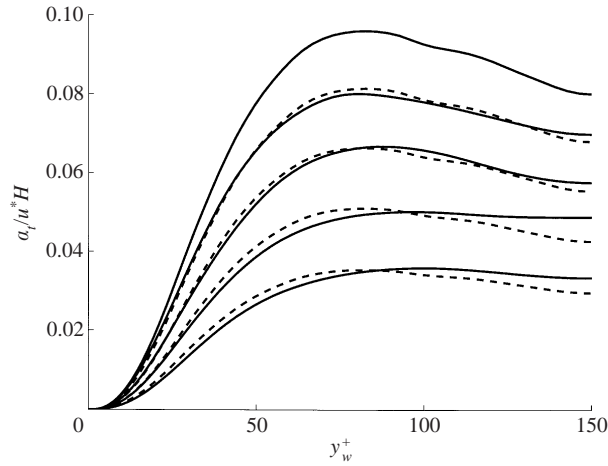


FIGURE 8. Turbulent conductivities. The solid lines indicate data obtained from the DNS at $Re_\tau = 150$; the dashed lines represent products of α_t/u^*H for $Pr = 1$ with the corresponding ratios $\alpha_t/(\alpha_t|_{Pr=1})$, given in figure 10. Turbulent conductivity increases monotonically with Pr over the whole channel height, and is plotted for $Pr = 0.025, 0.05, 0.1, 0.3, 1.0$.

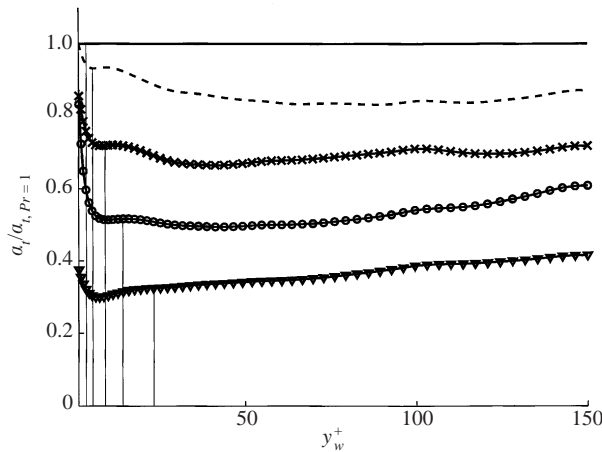


FIGURE 9. Profiles of $\alpha_t/\alpha_{t,Pr=1.0}$, at different values of the Prandtl number, evaluated from DNS at $Re_\tau = 150$. ∇ , $Pr = 0.025$; \ominus , $Pr = 0.05$; \times , $Pr = 0.1$; $---$, $Pr = 0.3$; $---$, $Pr = 1.0$.

Turbulent diffusivities, α_t , were calculated from the DNS by using equation (2.3). These are plotted as solid lines in figure 8. A monotonic decrease with decreasing Prandtl numbers is observed at all y/H . The ratio of α_t to the value obtained for $Pr = 1$ is shown in figure 9. The edges of the conductive sublayer are indicated by the vertical lines. An approximate representation of these curves, from the viewpoint of making practical calculations, is to use the average values for locations outside the conductive sublayer, $\langle \alpha_t \rangle$. These averaged results are summarized in table 1 and plotted in figure 10 as the ratio of $\langle \alpha_t \rangle$ to the value of $\langle \alpha_t \rangle$ for $Pr = 1$. The curve in this figure represents the equation

$$\frac{\langle \alpha_t \rangle}{\langle \alpha_t \rangle_{Pr=1}} = 1 - \exp(-C Pe_\tau^n) \tag{4.9}$$

with $C = 0.232$ and $n = 0.574$. The dashed curves in figure 8 are the calculated

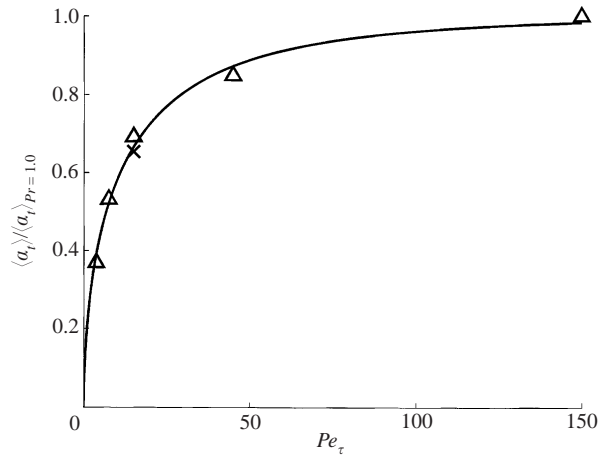


FIGURE 10. Ratio of averaged turbulent conductivities for $Re_\tau = 150$ at a given Prandtl number, to the average at $Pr = 1.0$. Δ , DNS data; —, equation (4.9). The cross is for a calculation at $Re_\tau = 300$, $Pr = 0.05$. Averaging has been applied only in the region outside the conductive sublayer.

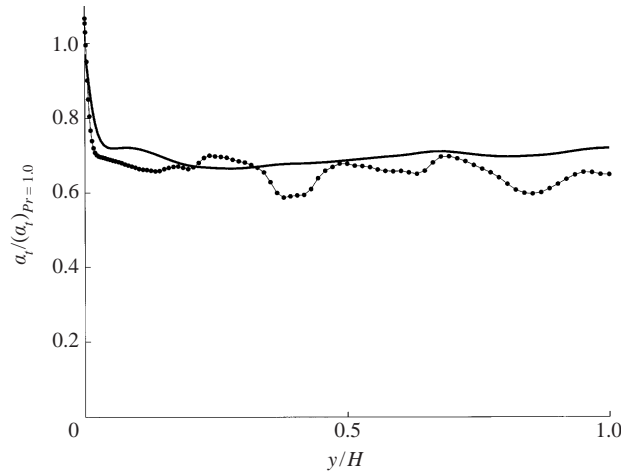


FIGURE 11. Ratio of turbulent conductivity at a given Pr with the value for $Pr = 1.0$, at the same Re_τ . The solid line represents $Re_\tau = 150$ and the dots $Re_\tau = 300$. The Péclet number has the same value ($Pe_\tau = 15$) for both curves.

values of $\langle \alpha_t \rangle$ that are obtained by using the measurements at $Pr = 1$ and the ratios $\langle \alpha_t \rangle / \langle \alpha_t \rangle_{Pr=1}$. A rough fit is observed. The values of $\langle \alpha_t \rangle / \langle \alpha_t \rangle_{Pr=1}$ in table 1 were used to calculate temperature profiles and values of Nu_c . Excellent agreement with the DNS is observed in figures 2 and 4, so the rough approximation of $\langle \alpha_t \rangle$ does not translate into significant errors in making heat-transfer calculations.

The main results presented in figures 4, 5 and 10 were obtained at a single Reynolds number, $Re_\tau = 150$, so the use of $Pe_\tau = Re_\tau Pr$ in these figures could be criticized because it suggests a generality which was not explored. Some support for this type of plot can be obtained because heat transfer data represented by (4.8) were obtained over a range of Reynolds numbers.

Of more interest are DNS of heat transfer at $Re_\tau = 300$ that are currently under

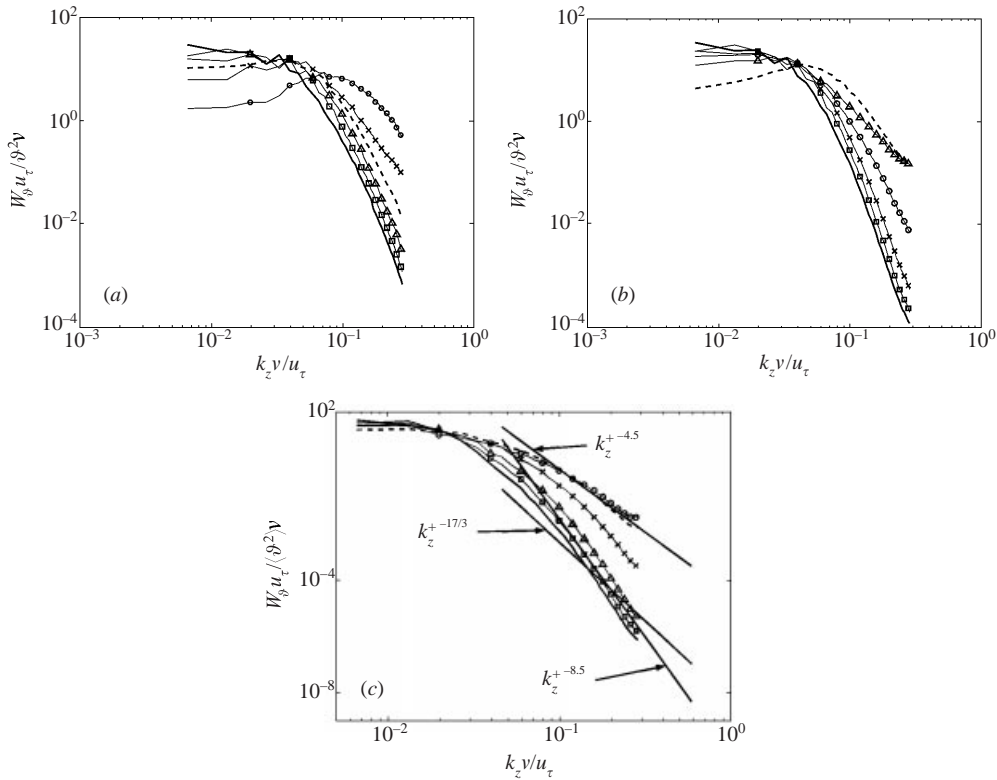


FIGURE 12. Spanwise temperature and wall-normal velocity spectra at (a) $y^+ = 10$, (b) $y^+ = 41$ and (c) $y^+ = 150$. \ominus —, v' -spectrum; —, ϑ' -spectrum at $Pr = 0.025$; \square —, ϑ' -spectrum at $Pr = 0.05$; \triangle —, ϑ' -spectrum at $Pr = 0.1$; \dashv —, ϑ' -spectrum at $Pr = 0.3$; \times —, ϑ' -spectrum at $Pr = 1.0$. Solid lines in (c) indicate slopes that are discussed in the paper.

way. These have not fully converged so a detailed account of the results is not justified. However, a discussion of the values of eddy diffusivity being calculated is of interest. Values of $\alpha_t/(\alpha_t|_{Pr=1})$ for $Pr = 0.05$ and $Re_\tau = 300$ ($Pe_\tau = 15$) are plotted as points in figure 11. The solid curve represents the calculations for $Pr = 0.1$ and $Re_\tau = 150$ ($Pe_\tau = 15$). Good agreement is noted. In fact the average values of the ratio over the region $y^+ > 8$ are 0.69 for $Re_\tau = 150$ and 0.66 for $Re_\tau = 300$ (plotted as a cross in figure 10). Values of Nu_c and Nu_b obtained with this DNS at $Re_\tau = 300$ are presented in figures 4 and 5. These also show good agreement with results obtained for $Re_\tau = 150$.

4.3. Spectra

Spanwise one-dimensional spectra of the temperature fluctuations are presented in figures 12(a) to 12(c) for different distances from the wall. The ordinate is $W_{\theta} u_{\tau} / \vartheta^2 \nu$, so the areas under the curves equal unity. For comparison the non-dimensional spectral density function for v^2 is also given. A striking feature in all of these spectra is the sharp drop in W_{θ} at large k_z from what is observed at $Pr = 1$. Decreases of the effectiveness of high-wavenumber velocity fluctuations in creating temperature fluctuations are clearly seen for decreasing Pr . Table 2 lists median wavenumbers, along with η_g^+ , ε_g^+ , ε^+ and η^+ .

The one-dimensional spectral density functions for $\overline{v^2}$ show definite maxima at

Pr	η_g^+	η^+	$\varepsilon_g^+ \times 10^4$	$\varepsilon^+ \times 10^4$	$k_{z\ m}^+$ for W_{vv}^+	$k_{z\ m}^+$ for $W_{g_g}^+$	$\frac{\overline{\partial^2 u_\tau}}{\varepsilon_g H}$	y^+
0.025	27.3	1.7	9.8	1158.0	0.094	0.017	0.361	10
	34.2	2.2	18.0	466.9	0.052	0.014	0.655	41
	43.7	2.7	22.6	175.5	0.035	0.010	0.967	76
	58.1	3.7	22.5	56.1	0.019	0.007	1.540	150
0.05	16.2	1.7	38.7	1158.0	0.094	0.022	0.154	10
	20.4	2.2	73.8	466.9	0.052	0.017	0.435	41
	26.0	2.7	88.7	175.5	0.035	0.012	0.652	76
	34.6	3.7	86.8	56.1	0.019	0.009	0.999	150
0.1	9.6	1.7	120.4	1158.0	0.094	0.030	0.056	10
	12.1	2.2	214.9	466.9	0.052	0.022	0.251	41
	15.4	2.7	235.7	175.5	0.035	0.014	0.405	76
	20.5	3.7	236.9	56.1	0.019	0.010	0.627	150
0.3	4.2	1.7	467.5	1158.0	0.094	0.037	0.029	10
	5.3	2.2	559.6	466.9	0.052	0.025	0.172	41
	6.8	2.7	480.4	175.5	0.035	0.018	0.294	76
	9.0	3.7	486.3	56.1	0.019	0.012	0.487	150
1.0	1.7	1.7	1531.5	1158.0	0.094	0.046	0.015	10
	2.2	2.2	907.0	466.9	0.052	0.032	0.112	41
	2.7	2.7	608.4	175.5	0.035	0.022	0.201	76
	3.7	3.7	545.0	56.1	0.019	0.013	0.315	150

TABLE 2. Parameters characterizing the spectral density function of temperature fluctuations.

$k_z^+ > 0$ for $y_w^+ = 10$ and 41 and a very weak maximum for $y_w^+ = 76$ (not shown here). This results because of the influence of streamwise vortices, which increase in size with the distance from the wall. Measurements of W_{g_z} for $Pr = 1$ show a less pronounced maximum. Maxima are not observed at very small Pr , indicating that thermal conductivity is diminishing the importance of the wall vortices.

Since the spectrum for $\overline{v^2}$ at $y_w^+ = 150$ is approximately the same as W_{g_z} for $Pr = 1$, the role of molecular diffusivity in damping large-wavenumber temperature fluctuations is more clearly seen at this location. A line with a slope of $k_z^{+17/3}$ is shown in figure 12(c). This corresponds to the prediction by Batchelor *et al.* (1959) in the limit of large $k\eta_g$ for the inertial-diffusive subrange of homogeneous, isotropic turbulence. The drop-off of the $W_{g_z}(k_z)$ spectrum at large k_z^+ is sharper than $k_z^{+17/3}$. This behaviour can be explained because the Reynolds number is too small to have an extended range of k_z where $W_{v_z} \approx k_z^{-5/3}$. A more realistic approach is to use equation (2.10d) with W obtained from the DNS calculations. Figures 13(a) and 13(b) show plots of $W_{g_z} \alpha^3 k_z^4 / W_{v_z} \varepsilon_g$. The results for $Pr = 0.025, 0.05$ and 0.1 show a plateau at the highest resolved wavenumbers. The lines in figure 13 indicate a value of $k_z \eta_g = 3.0$. This roughly defines the wavenumber at which a limiting behaviour, defined by equation (2.10d), commences. As indicated in figure 12(c), $W_{v_z}(k_z)$ varies as $k_z^{-4.5}$ at large wavenumbers. Thus, in accordance with equation (2.10d), $W_{g_z}(k_z)$ should vary as $k_z^{-8.5}$, as shown in figure 12(c).

Similar results are obtained for streamwise spectra $W_{g_x}(k_x)$. Figure 14 shows a plot of $W_{g_x}(k_x) u_\tau / \overline{\partial^2 v}$ obtained at $y^+ = 150$. A damping of high-wavenumber fluctuations is noted at large k_x . Figure 15 plots $W_{g_x} \alpha^3 k_x^4 / W_{v_x} \varepsilon_g$ versus $k_x \eta_g$. A plateau at large k_x

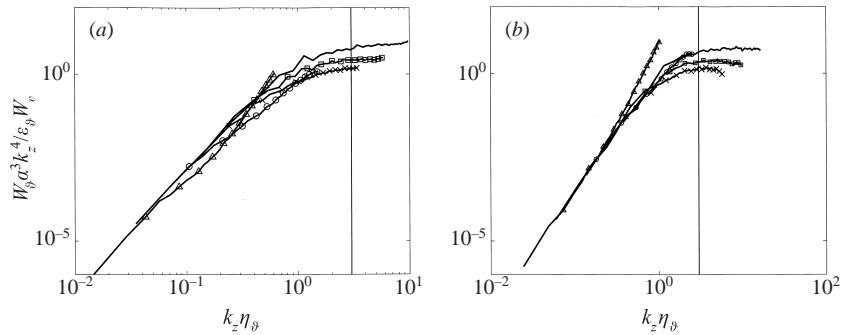


FIGURE 13. Spanwise temperature spectra at (a) $y_w^+ = 41$, (b) $y_w^+ = 150$. The scaling is consistent with equation (2.10d). The vertical line corresponds to $k_z \eta_\theta = 3.0$. —, \mathcal{G}' -spectrum at $Pr = 0.025$; $-\square-$, \mathcal{G}' -spectrum at $Pr = 0.05$; $-\times-$, \mathcal{G}' -spectrum at $Pr = 0.1$; $-\circ-$, \mathcal{G}' -spectrum at $Pr = 0.3$; $-\triangle-$, \mathcal{G}' -spectrum at $Pr = 1.0$.

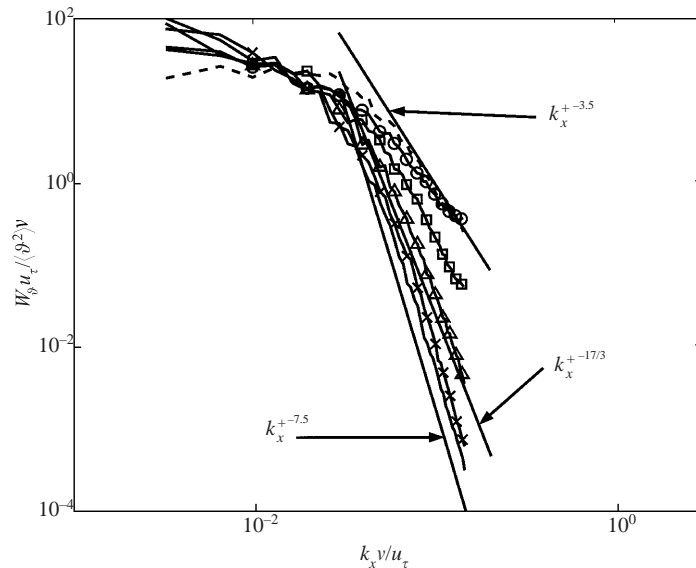


FIGURE 14. Streamwise temperature spectra at $y_w^+ = 150$. Solid lines indicate slopes discussed in the paper. ---, v' -velocity spectrum; —, \mathcal{G}' -spectrum at $Pr = 0.025$; $-\times-$, \mathcal{G}' -spectrum at $Pr = 0.05$; $-\triangle-$, \mathcal{G}' -spectrum at $Pr = 0.1$; $-\square-$, \mathcal{G}' -spectrum at $Pr = 0.3$; $-\circ-$, \mathcal{G}' -spectrum at $Pr = 1.0$.

begins at $k_x \eta_\theta$ approximately equal to 3.0. The slope of the $W_{v_x}(k_x)$ spectrum at large k_x^+ has a smaller negative value ($k_x^+^{-3.5}$) than is observed for $W_{v_z}(k_z)$. This accounts for the closer agreement with a $k_x^+^{-17/3}$ asymptote, observed in figure 14.

4.4. Mean-square fluctuations and correlation coefficients

Figure 16 shows calculated values of the root-mean-square of temperature fluctuations. As was done in figure 7, for the term representing Reynolds transport, $\overline{\mathcal{G}^2}$ is made dimensionless with $T_w - T_c$. The change in the $\mathcal{G}' = \overline{\mathcal{G}^2}^{1/2}$ profile with changes of Pr from 1 to 0.3 can be understood by using mixing-length arguments whereby \mathcal{G}' should scale with the product of the mixing length and the gradient in the mean temperature. The increase in \mathcal{G}' in the centre regions of the channel, therefore, can be ascribed to

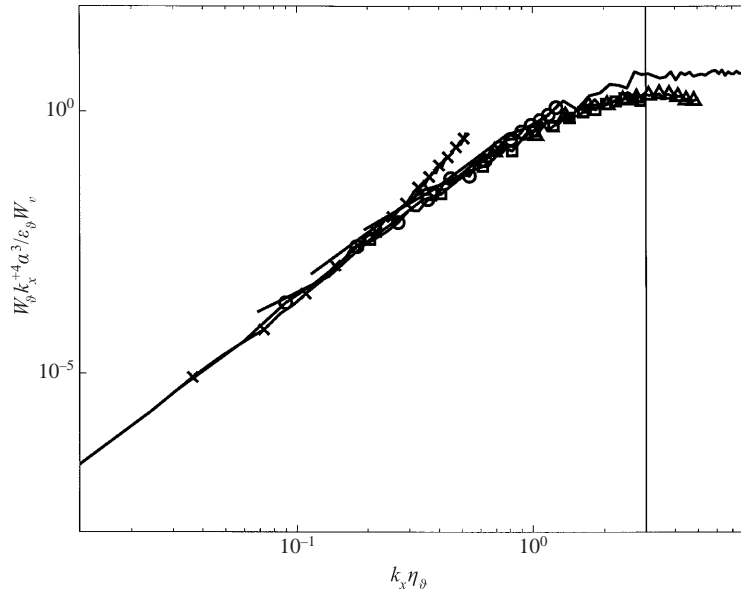


FIGURE 15. Streamwise temperature spectra at $y_w^+ = 150$. The scaling is consistent with equation (2.10d). The vertical line correspond to $k_x \eta_\theta = 3.0$. Temperature streamwise wavenumber spectra at $y_w^+ = 150$. Solid lines indicate slopes discussed in the paper. —, \mathcal{G}' -spectrum at $Pr = 0.025$; \triangle , \mathcal{G}' -spectrum at $Pr = 0.05$; \square , \mathcal{G}' -spectrum at $Pr = 0.1$; \circ , \mathcal{G}' -spectrum at $Pr = 0.3$; \times , \mathcal{G}' -spectrum at $Pr = 1.0$.

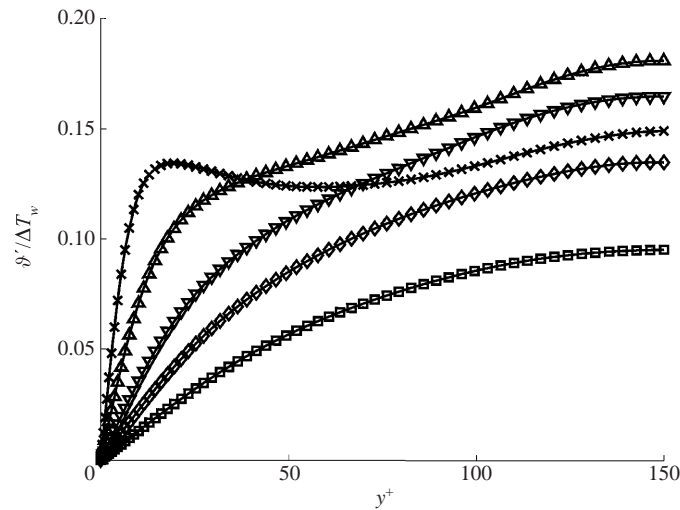


FIGURE 16. Standard deviations of temperature fluctuations scaled by the temperature difference between wall and centreline. \times , $Pr = 1.0$; \triangle , $Pr = 0.3$; ∇ , $Pr = 0.1$; \diamond , $Pr = 0.05$; \square , $Pr = 0.025$.

an increase in dT/dy . The decrease in \mathcal{G}' close to the wall results from the decrease in dT/dy .

An understanding of the monotonic decrease of \mathcal{G}' from $Pr = 0.3$ to $Pr = 0.025$ can be obtained from the results on spectra. These show that, with decreasing Pr (or increasing thermal conductivity), the temperature field loses its ability to respond to

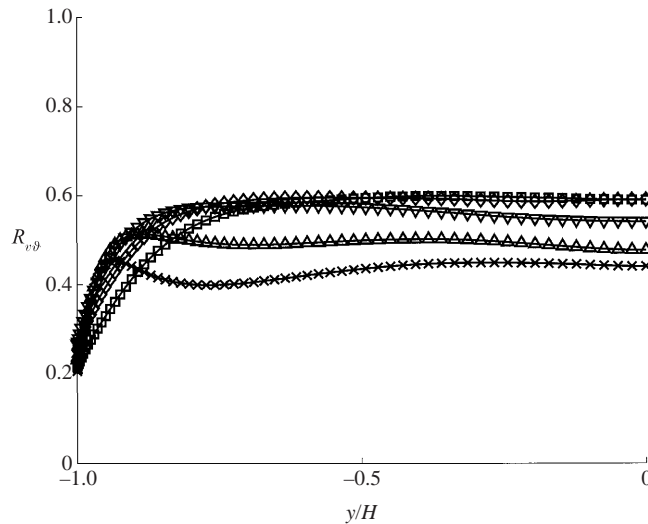


FIGURE 17. Correlation coefficient between wall-normal velocity component and temperature fluctuations. \times —, $Pr = 1.0$; \triangle —, $Pr = 0.3$; ∇ —, $Pr = 0.1$; \diamond —, $Pr = 0.05$; \square —, $Pr = 0.025$.

large-wavenumber velocity fluctuations. As a result, there is a decrease in \mathcal{G} because, effectively, the temperature field sees a turbulent velocity field with smaller intensities. This interpretation of figure 16 is consistent with the results on $\overline{v\vartheta}$ in figure 7. These show an increase in $\overline{v\vartheta}/u_\tau\Delta T_c$ from $Pr = 1$ to $Pr = 0.3$ and a decrease from $Pr = 0.1$ to $Pr = 0.025$.

Values of the correlation coefficient $R_{v\vartheta} = \overline{v\vartheta}/v'\mathcal{G}$ are presented in figure 17. These show a small range of values (0.4 to 0.6) outside the conductive sublayer. An understanding of the influence of Pr on the results in figure 17 can be obtained by recognizing that the damping of high-wavenumber contributions to $W_{\vartheta_i}(k_i)$ means that the temperature fluctuations are associated with lower-wavenumber velocity fluctuations. This appears to increase the correlation between the temperature and the velocity fluctuations, leading to an increase in $R_{v\vartheta}$. However the damping can also mean that the temperature field effectively sees only that part of the velocity field that is characterized by low wavenumbers. This would lead to smaller $R_{v\vartheta}$.

In order to investigate further the behaviour of $R_{v\vartheta}$, we performed a quadrant analysis for the turbulent heat flux. First- and third-quadrant events contribute positively to the turbulent heat flux, while second- and fourth-quadrant events make negative contributions. Figure 18 shows probabilities of events in each quadrant, averaged over $-0.12 \leq y/H \leq 0.12$. It is noted that, as Pr increases, the probability of positive contributions to the turbulent heat flux decreases, while the probability of negative contributions increases. This is consistent with the observed decrease of $R_{v\vartheta}$ with increasing Pr .

Correlation coefficients $R_{u\vartheta}$ are presented in figure 19. Kim & Moin (1989) showed that flow-oriented vortices control both the u and ϑ fluctuations close to the wall for $Pr = 1$. As has already been noted in the previous subsection these wall vortices play a less important role at small Pr . This accounts for the decrease in $R_{u\vartheta}$ for decreasing Pr .

As discussed in §2.2, a decrease in the effectiveness of large-wavenumber contributions of velocity fluctuations to three-dimensional spectra of the temperature fluctuations can be expected at small Pr . The spectral density function includes the

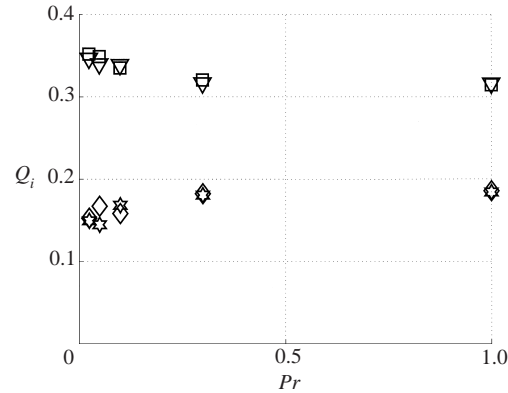


FIGURE 18. Probabilities of $v'g'$ quadrant events, averaged over a region extending from $y/H = -0.12$ to $y/H = 0.12$ across the centreline. \square , $v' > 0$, $g' > 0$; \diamond , $v' < 0$, $g' > 0$; ∇ , $v' < 0$, $g' < 0$; \star , $v' > 0$, $g' < 0$.

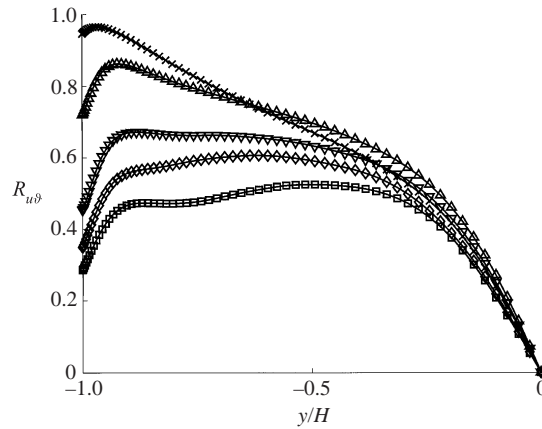


FIGURE 19. Correlation coefficient between streamwise velocity component and temperature fluctuations. $-\times-$, $Pr = 1.0$; $-\triangle-$, $Pr = 0.3$; $-\nabla-$, $Pr = 0.1$; $-\diamond-$, $Pr = 0.05$; $-\square-$, $Pr = 0.025$.

concept of temperature. The use of a friction temperature to make it dimensionless produces very large decreases with decreasing Pr , because of the increase of q_w . Figure 12 avoids this difficulty by using $\overline{\mathcal{G}^2}$ as a scaling function. This more clearly shows the effect of Pr and also allows a comparison with velocity spectra, such as shown in figure 12. However, since the areas under these curves equal unity, the spectral density functions show a decrease with decreasing Pr at large k_i and an increase at small k_i . The use of ε_g as a scaling function could be a better choice to show the influence of Pr . Since ε_g is approximately equal to production, $P_g = \overline{v\mathcal{G}d\bar{T}/dy}$, except for locations very close to the wall, it reflects the effects of local changes of $d\bar{T}/dy$ with Pr . This is illustrated in the plots of $W_{g_z}(k_z)$ at $y^+ = 150$ for different Pr in figure 20. The areas under these curves, reported in table 2, are equal to $\overline{\mathcal{G}^2}u_\tau/\varepsilon_g H$, rather than unity. Figure 20 clearly shows the effect of damping of high-wavenumber fluctuations on the one-dimensional spectral function $W_{g_z}(k_z)$. We see a decrease in $W_{g_z}(k_z)$ at all k_z and a sharp drop-off at large k_z . The values of $\varepsilon_g v/u_\tau^2 T_w^2$ used in developing figure 20 are shown in figure 21.

The damping of large-wavenumber temperature fluctuations is illustrated in the

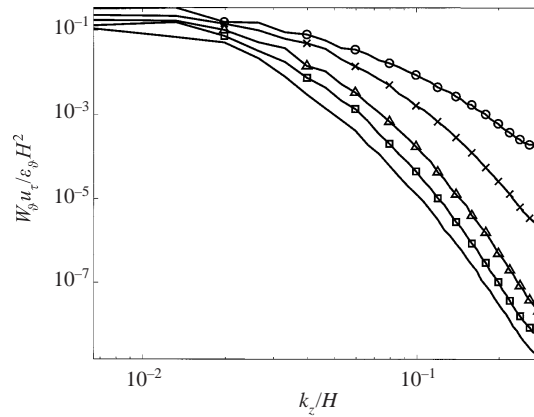


FIGURE 20. Spanwise spectrum for temperature fluctuations at $y^+ = 150$, scaled by the dissipation of temperature fluctuations. \circ —, $Pr = 1.0$; \times —, $Pr = 0.3$; \triangle —, $Pr = 0.1$; \square —, $Pr = 0.05$; —, $Pr = 0.025$.

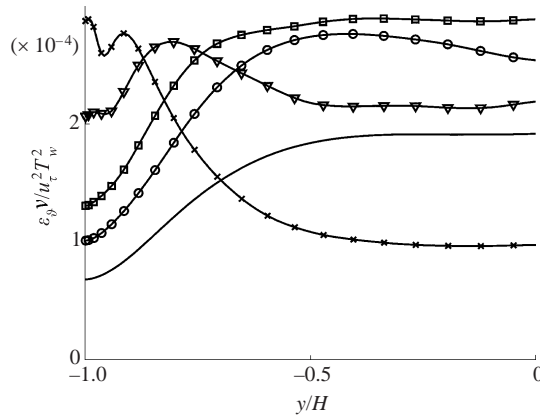


FIGURE 21. Dissipation of $\theta^2/2$, scaled as $\epsilon_\theta v / u_\tau^2 T_w^2$. \times —, $Pr = 1.0$; ∇ —, $Pr = 0.3$; \square —, $Pr = 0.1$; \circ —, $Pr = 0.05$; —, $Pr = 0.025$.

plots of temperature contours in the (y, z) -plane, given in figure 22(b, d). These clearly show an increase in the size of the structures in the temperature field and a smoothing of contours of constant temperature with decreasing Pr . For comparison, figure 22(a) gives contours of the streamwise velocity fluctuations calculated at the same (y, z) -plane and at the same time for which figure 22(b, c) were calculated. It is interesting to note that, in accordance with the strong reduction in $R_{u\theta}$ with decreasing Pr , there is no similarity between u' and θ' contours, at $Pr = 0.025$ and 0.1. At $Pr = 1$, however, a similarity is noted in the near-wall region. In the core region, no similarity can be expected even at $Pr = 1$, since the different boundary conditions imposed on u' and θ' cause the production of u' to vanish and the production of θ' to reach a local maximum at the centreline. These differences are manifested in the more intense fluctuations in figure 22(d), when compared with figure 22(a).

The theory of Batchelor *et al.* (1959) helps in interpreting these results. The calculations from the DNS agree with their suggestions that a drop-off at $k_z \approx \eta_\theta^{-1}$ occurs and that equation (2.10d) describes the limiting behaviour at large k_z .

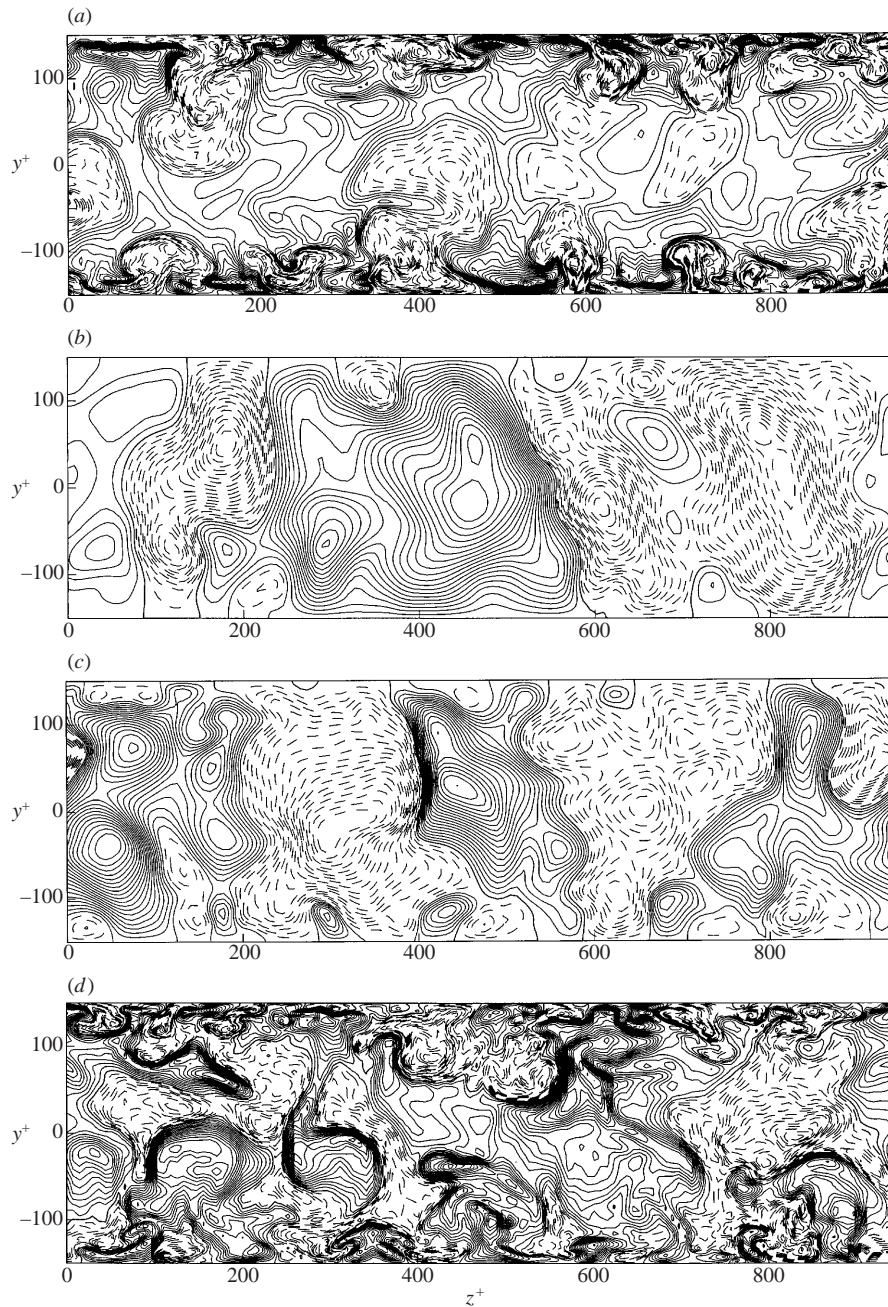


FIGURE 22. Temperature and velocity fluctuations on a cross-flow plane. Solid lines indicate positive fluctuations, while dashed lines indicate negative fluctuations. Fields in (a)–(c) are evaluated at the same time and location: (a) streamwise velocity; (b) temperature, $Pr = 0.025$; (c) temperature, $Pr = 0.1$; (d) temperature, $Pr = 1.0$.

5. Discussion

As the molecular thermal diffusivity increases, the effectiveness of high-wavenumber velocity fluctuations in creating scalar turbulence decreases. Thermal diffusivity acts as a filter that, effectively, decreases the magnitude and increases the length scale of the velocity fluctuations ‘seen’ by the scalar field. A principal contribution of this paper is the demonstration of this filtering and the provision of an interpretation which uses results obtained for homogeneous isotropic turbulence. In particular, the thermal microscale, η_θ , is used to define the influence of Prandtl on the ‘cut-off’ wavenumber. The comparison is not meant to provide a confirmation of theories in the literature, because the flow is non-homogeneous and the Reynolds number is too low for an inertial subrange in the velocity spectrum to exist.

A number of researchers (Reynolds 1975) have interpreted the decrease of turbulent diffusivity with decreasing Prandtl number as resulting from a decrease of the mixing length because of a leakage of the transported quantity from eddies by molecular diffusion. The present paper offers an alternative interpretation which looks upon the turbulent diffusivity as being proportional to the product of a time scale and the variance of the velocity fluctuations responsible for transporting heat. The decrease in turbulent diffusivity because of increasing molecular diffusion can, therefore, be interpreted as being a consequence of a filtering action which causes a decrease in the magnitude of the velocity fluctuations responsible for transporting heat. Furthermore, there is also a decrease in the Lagrangian time scale because molecular diffusivity causes thermal markers to escape from transporting eddies.

Figure 7 shows an increase in $\overline{v\theta}$ with a decrease from $Pr = 1$ to $Pr = 0.1$. If one uses mixing-length arguments \mathcal{G}' can be presumed to increase with $l d\bar{T}/dy$. In the central region of the channel cross-section, $d\bar{T}/dy$ increases when Pr decreases from 1 to 0.3. This would, therefore, tend to cause an increase in $\overline{v\theta}$. However, close to the wall $d\bar{T}/dy$ decreases with a change of Pr from 1 to 0.3. Consequently, a decrease in $\overline{v\theta}$ should be expected in this region. Changes in $\overline{v\theta}$ with a decrease of Pr from 0.1 to 0.025 appear to be associated, mainly, with the filtering effect of molecular thermal diffusivity. The decrease in $\overline{v\theta}$, observed at all y^+ , is caused by a decrease in the effectiveness of velocity fluctuations, in generating temperature fluctuations, with decreasing Pr , as shown in figure 22.

The influence of $d\bar{T}/dy$ on $\overline{v\theta}$ can be taken, partially, into account by defining turbulent diffusivities. These are found to decrease monotonically with decreasing Pr at all locations in the channel. These results are consistent with studies of diffusion from a point source in isotropic turbulence by Saffman (1960, 1963) and by Kontomaris & Hanratty (1993) and with studies by Kontomaris & Hanratty (1994) of point source diffusion in a DNS of channel flow.

The finding that $\langle\alpha_t\rangle/\langle\alpha_t\rangle_{Pr=1}$ does not show large variations with y^+ outside the conductive sublayer suggests a good way to approximate the average temperature field. This has been tested by calculating the temperature fields by using α_t obtained from a relation that provides $\langle\alpha_t\rangle/\langle\alpha_t\rangle_{Pr=1}$ as a function of Pe_τ . See figures 2, 4, 9.

The usual practice in calculating turbulent temperature fields at different Prandtl numbers is to develop a model for the turbulent viscosity and to define a turbulent Prandtl number which can depend on spatial location and on the molecular Prandtl number. The results shown in figures 9, 10, 11 suggest that it might be advantageous to calculate the effect of Pr on the temperature field by using a model for the turbulent diffusivity of heat for $Pr = 1$ rather than the turbulent viscosity. This is done in figure 4 for $Re_\tau = 150$ and for $Re_\tau = 300$.

The large changes of α_t , observed for small Pr , occur in situations in which molecular transport is dominating turbulent transport. Consequently, the decreases in the turbulent diffusivity do not have a strong effect on the mean temperature field. Even by assuming $\alpha_t = \alpha_{tPr=1}$, the maximum relative error in the calculation of the Nusselt number for $Pr = 0.05$ via equation (2.4b) is not larger than 17%.

6. Conclusions

The principal results of this study are contained in figures 8, 9, 12, 20 and 22. The first of these shows a monotonic decrease in α_t with decreasing Pr at all y^+ . The second shows only small variations of $\langle\alpha_t\rangle/\langle\alpha_t\rangle_{Pr=1}$ over all locations in the channel that are outside the conductive sublayer. The last three show sharp decreases in W_g beyond $k_z, k_x \approx 3.0\eta_g^{-1}$, where η_g increases with decreasing Pr . Molecular diffusivity acts as a filter by decreasing the effectiveness of large-frequency velocity fluctuations in creating temperature fluctuations. This, in turn, causes the observed decrease in α_t .

The support and facilities of the National Center for Supercomputing Applications at the University of Illinois at Urbana-Champaign and financial support from the University of Trieste are gratefully acknowledged.

REFERENCES

- BATCHELOR, G. K. 1959 Small-scale variation of convected quantities like temperature in turbulent fluid. Part I. General discussion and the case of small conductivity. *J. Fluid Mech.* **5**, 113–133.
- BATCHELOR, G. K., HOWELLS, I. D. & TOWNSEND, A. A. 1959 Small-scale variation of convected quantities like temperature in turbulent fluid. Part II. The case of large conductivity. *J. Fluid Mech.* **5**, 134–139.
- BROOKE, J. W. 1994 Transport processes in a direct numerical simulation of turbulent channel flow. PhD thesis, University of Illinois, Urbana.
- CLAY, J. P. 1973 Turbulent mixing of temperature in water, air and mercury. PhD thesis, University of California, San Diego.
- CORCORAN, W. H., PAGE, F. J., SCHLINGER, W. G. & SAGE, B. H. Temperature and velocity distribution in uniform flow between parallel plates. *Indust. Engng Chem.* **44**, 419–424.
- CORRSIN, S. 1951 On the spectrum of isotropic temperature fluctuations in an isotropic turbulence. *J. Appl. Phys.* **22**, 469.
- GIBSON, C. H. 1968a Fine structure of scalar field mixed by turbulence. I: zero-gradient points and minimal gradient surfaces. *Phys. Fluids* **11**, 2305–2315.
- GIBSON, C. H. 1968b Fine structure of scalar field mixed by turbulence. II: Spectral theory. *Phys. Fluids* **11**, 2316–2327.
- HINZE, J. O. 1975 *Turbulence*. McGraw-Hill.
- KASAGI, N. & IIDA, O. 1999 Progress in direct numerical simulation of turbulent heat transfer. In *Proc. Fifth ASME/JSME Joint Thermal Engng Conf.* (ed. D. L. Dwoyer & M. Y. Hussaini). Springer.
- KASAGI, N. & OHTSUBO, Y. 1993 Direct numerical simulation of low Prandtl number thermal field in a turbulent channel flow. In *Turbulent Shear Flow*, vol. 8 (ed. F. Durst *et al.*), pp. 97–119.
- KAWAMURA, H., ABE, H., MATSUO, Y. & YAMAMOTO, K. 1998 DNS of turbulent heat transfer in channel flow with respect to Reynolds number effect. In *Proc. Second EF Conf. on Turbulent Heat Transfer* (ed. D. L. Dwoyer & M. Y. Hussaini), vol. I, pp. 15–22. Springer.
- KIM, J. & MOIN, P. 1989 Transport of passive scalars in a turbulent channel flow. *Turbulent Shear Flows* **6**, 85–96.
- KONTOMARIS, K. & HANRATTY, T. J. 1993 Effect of molecular diffusivity in turbulent diffusion in isotropic turbulence. *Intl J. Heat Mass Transfer* **36**, 1403–1412.
- KONTOMARIS, K. & HANRATTY, T. J. 1994 Effect of molecular diffusivity on point-source diffusion in

- the centre of a numerically simulated turbulent channel flow. *Intl J. Heat Mass Transfer* **37**, 1817–1828.
- KNUDSEN, J. G. & KATZ, D. L. 1958 *Fluid Dynamics and Heat Transfer*. McGraw-Hill.
- LYONS, S. L., HANRATTY, T. J. & MCLAUGHLIN, J. B. 1991 Large-scale computer simulation of fully-developed channel flow with heat transfer. *Intl J. Numer. Meth. Fluids* **13**, 999–1028.
- NA, Y., PAPAVALIIOU, D. V. & HANRATTY, T. J. 1999 Use of direct numerical simulation to study the effect of Prandtl number on temperature fields. *Intl J. Heat Fluid Flow* **20**, 187–195.
- NIEDERSCHULTE, M. A., ADRIAN, R. J. & HANRATTY, T. J. 1990 Measurements of turbulent flow in a channel at low Reynolds numbers. *Expts Fluids* **9**, 222–230.
- OBUKHOV, A. M. 1949 Structura Temperaturogo polia v turbulentnom potoke. *Izv. Akad. Nauk. SSSR. Ser. Geofiz.* **13**, 59–63.
- PAGE, F. J., SCHLINGER, W. G., BREAU, D. K. & SAGE, B. H. 1952 Point values of eddy conductivity and viscosity in uniform flow between parallel plates. *Indust. Engng Chem.* **44**, 424–430.
- PAPAVALIIOU, D. V. & HANRATTY, T. J. 1997 Transport of a passive scalar in a turbulent channel flow. *Intl J. Heat Mass Transfer* **40**, 1303–1311.
- REYNOLDS, A. J. 1975 The prediction of turbulent Prandtl and Schmidt numbers. *Intl J. Heat Mass Transfer* **18**, 1055–1069.
- SAFFMAN, P. G. 1960 On the effect of molecular diffusivity in turbulent diffusion. *J. Fluid Mech.* **8**, 273–283.
- SAFFMAN, P. G. 1963 An approximate calculation of the Lagrangian auto-correlation coefficient for stationary homogeneous turbulence. *Appl. Sci. Res.* **IIA**, 245–255.
- TENNEKES, H. & LUMLEY, J. L. 1972 *A First Course in Turbulence*. MIT Press.